ORIGINAL ARTICLE

Relaxations of methylpyridinone tautomers at the C_{60} surfaces: DFT studies

Elahe Naderi¹; Mahmoud Mirzaei¹,*; Lotfollah Saghaie¹; Ghadamali Khodarahmi¹; Oğuz Gülseren²

¹Department of Medicinal Chemistry, School of Pharmacy and Pharmaceutical Sciences, Isfahan University of Medical Sciences, Isfahan, Iran

²Department of Physics, Faculty of Science, Bilkent University, Ankara, Turkey

Abstract

Density functional theory (DFT) based calculations have been performed to examine the relaxations of tautomers of 4–hydroxy–6–methylpyridin–2(1H)–one (MPO), as a representative of pyridinone derivatives, at the fullerene (C_{60}) surfaces. Optimized molecular properties including energies, dipole moments and atomic scale quadrupole coupling constants (C_Q) have been evaluated to investigate the structural and electronic properties of the models. The structural configurations of tautomers show different relaxations at the C_{60} surface yielding different magnitudes of total and binding energies. Moreover, deformation of each tautomer due to relaxation at the C_{60} surface with respect to the initial singular structure has been examined. Complimentary parameters of energy gaps and dipole moments exhibit the effects of relaxations at the C_{60} surface for the MPO counterparts. Atomic scale C_Q properties also indicate that the electronic properties of atoms show significant changes for tautomers and hybrid systems. As a final note, the tautomeric structures in singular and hybrid forms exhibit different electronic properties because of effects of interactions with C_{60}, especially for the interaction regions.

Keywords: *Density functional theory; Pyridinone; Quadrupole coupling constant; Tautomer.*

INTRODUCTION

Pyridinone derivatives are well known as iron chelators for pharmaceutical applications besides their biological activities in anti–HIV treatments [1–5]. 4–Hydroxy–6–methylpyridin–2(1H)–one (identified as MPO) (Fig. 1) is a representative of pyridinone derivatives with desired biological activities [6]. Tautomerization processes, which are common for heterocyclic organic compounds yielding structural deformations and different activities, could be occurred for MPO and related compounds [7-9]. In this case, recognitions of tautomeric structures are important in order to assign significant activities for desired compounds especially in biological treatments [10]. The stoichiometry of chemical structure is not changed in the tautomerization processes; therefore, recognition of an exact tautomer is not a simple task and it needs special methodologies and detectors. By introduction

of nanostructures, carbon based materials have been considered as essential compounds for several applications in biological systems [11-13]. Fullerene (C_{60}), nanotube, graphene, nanocone, nanorod and several other nanostructures have become subjects of several research studies to characterize their stabilities and activities [14-18]. Nanostructures have been also considered as proper carriers in targeted drug deliveries in order to reduce side effects of medicinal treatments for patients [19]. Covalent and non–covalent functionalizations of nanostructures by biological molecules for several purposes have been reported by earlier works [20-22]. Two molecular counterparts could be attached to each other through a molecular linkage or physical interactions [23, 24]. The carbon rings of nanostructures are full of electrons, which are proper sites for interactions with other atoms

* Corresponding Author Email: *mdmirzaei@pharm.mui.ac.ir*

and molecules. Accordingly, within this work, noncovalent functionalizations of C_{60} through relaxation of the original MPO and tautomers at the C_{60} surface (See Figs. 2 and 3) are explored based on quantum chemical computational methodologies. Stabilities and properties for three forms of MPO structures including singular, separated and hybrid forms are investigated to identify the existence of tautomeric structures and their characteristic properties at the C_{60} surface.

To achieve this purpose, the optimized molecular properties and atomic scale electronic properties are evaluated for all investigated models of this work (Tables 1-4). In addition to atomic geometries, electronic properties of atoms are also very important to describe natures of chemical structures.

EXPERIMENTAL
Computational details

Structural models considered in this work are the original structures including C_{60}, MPO, and four tautomers (MPO–*i*) and their combinations to form MPO@C_{60} hybrids (See Figs. 2 and 3).
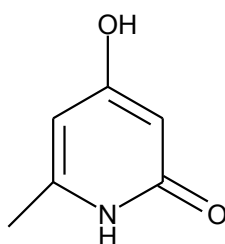

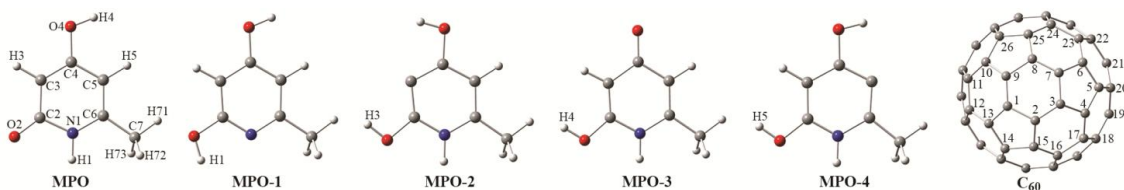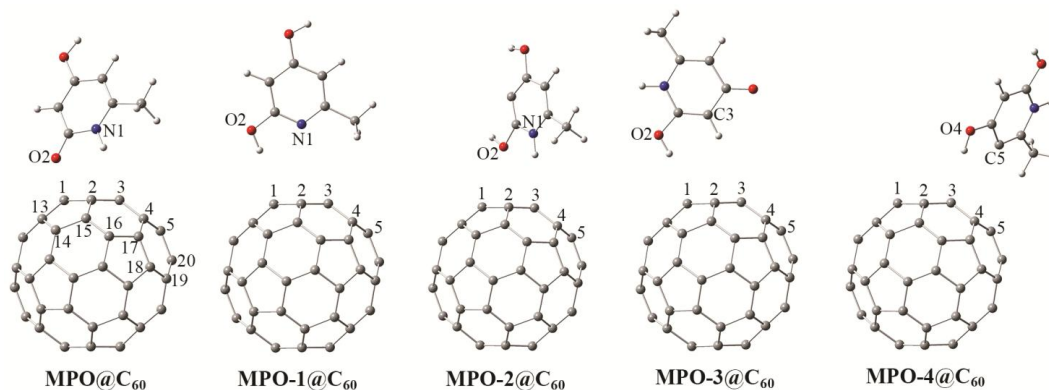Fig. 1: 4–hydroxy–6–methylpyridin–2(1H)–one (MPO) [6].

Fig. 2: Original singular models of MPO, tautomers and C_{60}.

Table 1: Physical properties from the optimized structures of 4–hydroxy–6–methylpyridin–2(1H)–one and tautomers*.

Property	MPO	MPO–1	MPO–2	MPO–3	MPO–4	C_{60}
Total Energy /eV	−11920.443 (−11920.442) [−74131.917]	−11920.387 (−11920.386) [−74131.839]	−11918.436 (−11918.435) [−74129.881]	−11920.067 (−11920.066) [−74131.547]	−11918.004 (−11918.001) [−74129.484]	−62211.370
Deformation Energy /meV	0.884	0.838	0.879	1.366	3.328	—
Binding Energy /eV	−0.105	−0.082	−0.075	−0.111	−0.113	—
HOMO /eV	−5.673 (−5.664) [−5.728]	−6.256 (−6.249) [−5.993]	−4.941 (−4.948) [−4.859]	−5.728 (−5.714) [−5.568]	−4.497 (−4.431) [−4.715]	−5.987
LUMO /eV	−0.685 (−0.692) [−3.130]	−0.180 (−0.169) [−3.253]	−0.526 (−0.529) [−3.385]	−0.171 (−0.161) [−3.384]	−0.559 (−0.549) [−3.012]	−3.226
Energy Gap /eV	4.988 (4.972) [2.597]	6.077 (6.080) [2.740]	4.414 (4.419) [1.474]	5.556 (5.553) [2.184]	3.938 (3.881) [1.703]	2.761
Dipole Moment /Debye	6.232 (6.274) [5.602]	2.608 (2.553) [2.518]	3.731 (3.742) [4.487]	5.982 (6.029) [5.377]	4.301 (4.235) [6.362]	0.000

* See Figs. 2 and 3 for the numbers of atoms and models. In each row, the parameters are for singular, (separated), and [hybrid] models. The separated model is the extracted MPO molecule from the hybrid model.

Fig. 3: Relaxed tautomers of MPO at C_{60} surfaces, MPO–i@C_{60}.

Table 2: Quadrupole coupling constants (C_Q /kHz) for O, N, and C atoms of 4–hydroxy–6–methylpyridin–2(1H)–one and tautomers*.

Atom	MPO	MPO–1	MPO–2	MPO–3	MPO–4
	8598	9397	9092	9649	9675
O_2	(11247)	(9448)	(9094)	(9710)	(9685)
	[8467]	[9251]	[9075]	[9462]	[9676]
	9670	9612	8863	10119	8633
O_4	(12569)	(9610)	(8862)	(10126)	(8758)
	[9659]	[9611]	[8872]	[10083]	[8623]
	3255	3599	3018	4020	2922
N_1	(3253)	(3612)	(3015)	(4021)	(2911)
	[3159]	[3583]	[2893]	[4005]	[2925]
	2456	2222	2498	2061	2056
C_2	(2451)	(2221)	(2498)	(2056)	(2044)
	[2437]	[2206]	[2499]	[2054]	[2057]
	426	499	3716	363	348
C_3	(436)	(500)	(3711)	(366)	(356)
	[422]	[336]	[3691]	[358]	[342]
	2930	2973	3172	2932	3356
C_4	(2933)	(2971)	(3176)	(2932)	(3351)
	[2941]	[2976]	[3174]	[2947]	[3307]
	253	546	1032	1197	4122
C_5	(251)	(548)	(1031)	(1197)	(4186)
	[259]	[543]	[1019]	[1183]	[3942]
	2095	2336	2066	2257	2904
C_6	(2091)	(2333)	(2063)	(2255)	(2896)
	[2108]	[2329]	[2067]	[2235]	[2899]
	606	419	585	573	514
C_7	(606)	(417)	(586)	(571)	(512)
	[623]	[410]	[591]	[551]	[532]

* See Figs. 2 and 3 for the numbers of atoms and models. In each row, the parameters are for singular, (separated), and [hybrid] models. The separated model is the extracted MPO molecule from the hybrid model.

Table 3: Quadrupole coupling constants (C_Q /kHz) for H atoms of 4–hydroxy–6–methylpyridin–2(1H)–one and tautomers*.

Atom	MPO	MPO–1	MPO–2	MPO–3	MPO–4
H_1	250	278	248	255	246
	(248)	(276)	(244)	(255)	(246)
	[244]	[271]	[239]	[256]	[246]
H_3	206	205	273	204	202
	(206)	(205)	(272)	(206)	(202)
	[206]	[206]	[273]	[205]	[202]
H_4	291	290	270	289	259
	(291)	(290)	(269)	(282)	(263)
	[291]	[290]	[270]	[274]	[260]
H_5	204	201	203	204	288
	(204)	(202)	(203)	(204)	(288)
	[203]	[202]	[203]	[204]	[288]
H_{71}	196	195	195	196	197
	(196)	(195)	(195)	(196)	(198)
	[196]	[195]	[195]	[196]	[197]
H_{72}	190	193	190	190	190
	(190)	(193)	(191)	(190)	(190)
	[190]	[193]	[190]	[190]	[190]
H_{73}	190	193	190	190	190
	(190)	(193)	(191)	(190)	(190)
	[190]	[193]	[190]	[190]	[190]

* See Figs. 2 and 3 for the numbers of atoms and models. In each row, the parameters are for singular, (separated), and [hybrid] models. The separated model is the extracted MPO molecule from the hybrid model.

First, all individual structures are optimized to obtain their minimum energy configurations. Next, each of pre–optimized MPO counterparts are allowed to re–relax at the surface of frozen pre–optimized C_{60} counterpart in the hybrid structures. Optimized molecular properties including total energies, deformation energies, binding energies, energies of the highest occupied molecular orbital (HOMO) and the lowest unoccupied molecular orbital (LUMO), energy gaps, and dipole moments are extracted after the geometry optimization calculations (Table 1). The referred model systems during discussions of this works include singular, separated and hybrid models which stand for freestanding MPO structures, separated MPO structures after relaxation at the C_{60} surface, and MPO@C_{60} hybrid structures, respectively. In order to obtain the deformation energies, energy differences between the singular and separated structures are calculated; $E_{Deformation} =$ $E_{Separated,MPO} - E_{Isolated,MPO}$. The binding energies are obtained from energy differences between the separated and hybrid structures; $E_{Binding} = E_{MPO@C60} - E_{Separated,MPO} - E_{Isolated,C60}$. The energy gaps are energy differences between the HOMO and LUMO levels; $E_{Gap} = E_{LUMO} - E_{HOMO}$. Other parameters are directly calculated (i.e. reported by the optimization outputs). To better understand properties of the investigated systems, atomicscale quadrupole coupling constants (C_Q) are also obtained from the calculations of electric field gradient (EFG) tensors (q_{ii}; $|q_{zz}|>|q_{xx}|>|q_{yy}|$) for atoms of the optimized molecular systems [25]. EFG tensors, originated from the electronic sites of atoms, are sensitive to any perturbation to atomic chemical environments, which could be characterized by magnitudes of C_Q as interaction energies between the EFG and the nuclear quadrupole moment (Q) [25]. In order to calculate C_Q magnitudes, electric charge (e), Planck's constant (h), q_{zz}–eigenvalue

of the calculated EFG tensors, and the standard *Q* values for each type of atoms are used; C_Q (MHz) = $e^2Qq_{zz}h^{-1}$ [26-31]. All calculations of this work are performed by using the Gaussian 03 program based on density functional theory (DFT) and employing the B3LYP functional and the 6-31G* standard basis set and also including dispersion correction through employing IOp(3/124=3) for the interacting systems [32-34].

RESULTS AND DISCUSSION

Optimized molecular properties

The molecular properties of the obtained optimized structures of singular, separated and hybrid models as shown in Figs. 2 and 3 are presented in Table 1. The calculated total energies

indicated that the most stable structure is the original 4–hydroxyl model, in which MPO–2 and MPO-4 are both the least stable ones in all three cases of singular, separated and hybrid models. Note that the MPO molecules were extracted from the hybrid model and then their properties were regenerated and compared with the initial singular models. According to the results of optimizations, the orders of stabilities for MPO models are not changed in these three structural cases. The positive magnitudes of deformation energies, the energy differences of separated and singular models, indicate that the stabilities of all MPO models are slightly changes at the surface of C_{60} in comparison with their initial singular forms. The largest magnitudes of deformations

Table 4: Quadrupole coupling constants (C_Q /kHz) for C atoms of C_{60} counterparts*.

Atom	C_{60}	MPO@	MPO–1@	MPO–2@	MPO–3@	MPO–4@
C_1	1531	1503	1550	1548	1529	1459
C_2	1533	1563	1531	1560	1484	1555
C_3	1532	1476	1568	1493	1598	1548
C_4	1533	1522	1533	1506	1532	1581
C_5	1532	1522	1539	1508	1549	1584
C_6	1532	1476	1532	1494	1530	1625
C_7	1533	1534	1571	1434	1599	1740
C_8	1533	1571	1526	1624	1484	1376
C_9	1534	1616	1539	1538	1532	1597
C_{10}	1531	1614	1521	1535	1497	1529
C_{11}	1533	1513	1552	1542	1567	1524
C_{12}	1531	1548	1551	1552	1565	1489
C_{13}	1533	1505	1525	1517	1499	1535
C_{14}	1532	1538	1535	1529	1517	1542
C_{15}	1533	1530	1542	1523	1512	1518
C_{16}	1533	1534	1526	1547	1550	1530
C_{17}	1532	1526	1536	1542	1555	1517
C_{18}	1533	1530	1533	1532	1529	1521
C_{19}	1531	1528	1534	1538	1546	1533
C_{20}	1533	1526	1531	1541	1535	1515
C_{21}	1532	1534	1534	1538	1547	1508
C_{22}	1532	1529	1532	1531	1527	1532
C_{23}	1532	1562	1536	1554	1555	1503
C_{24}	1532	1504	1525	1559	1548	1475
C_{25}	1533	1616	1539	1536	1512	1561
C_{26}	1532	1616	1533	1539	1518	1542

* See Figs. 2 and 3 for the numbers of atoms and models. C_{60} implies for the singular model and the others imply for the hybrid forms.

are observed for the MPO-3 and MPO-4 models. The magnitudes of binding energies, the energy differences between hybrids and their individual components, indicate that binding affinities of two components are different in the hybrid models. The orders of favorability of counterparts to bind each other are different following the order as MPO–4 > MPO–3 > MPO > MPO–1 > MPO–2. The energies for HOMO and LUMO levels indicate that the higher levels do not experience significant effects of hybridizations whereas the lower levels affected significantly in the hybrid systems. Indeed, C_{60} plays a modulator role for the HOMO and LUMO levels of MPO counterparts in the hybrid systems. Interestingly, the magnitudes of energy gaps are mostly similar to the band gap of free C_{60} model. Different polarities with significant changes in the hybrid systems are also observed for the models of this study. As a conclusion of this section, although the orders of stabilities for the investigated models systems are similar in all three cases, the magnitudes of deformations energies and binding energies exhibit some different points about the optimized model structures. Moreover, the energy gaps show significant effects of hybridizations for the investigated model systems especially for the LUMO levels whereas the relaxed separated models demonstrate almost similar properties to initial singular MPO models.

Atomic scale quadrupole coupling constants

Quadrupole coupling constants (C_Q) are originated from the electronic sites of atoms; therefore, they are useful to investigate electronic properties of matters. Tables 2 – 3 include the magnitudes of C_Q properties for atoms of the optimized structures in different cases (Figs. 2 and 3). The oxygen atoms of MPO models, O_2 and O_4, are in different chemical environments due to their different structural characteristics to be in enol or in keto forms and also directions of O–H bonds in enol forms. The MPO counterparts show different relaxations at the surfaces of C_{60}, but one oxygen atom of MPO is always close to the C_{60} substrate. The only nitrogen atom of MPO structures detects the effects of relaxations and hybridizations among model systems. Lone pairs of electrons in valance shells of nitrogen and oxygen atoms are important to detect effects on the atomic sites of the system. Carbon atoms do not have lone pairs of electrons; however, their atomic sp^2 hybridizations versus stable sp^3 hybridizations almost keep them as active

atoms in monitoring the electronic properties of matters. Due to this trend, the contributions of hydrogen atoms of carbon atoms of heterocyclic ring of MPO (H_3 and H_5) to tautomerization processes have been considered to determine the tautomeric forms of this work. Due to electronic origination of C_Q properties, the magnitudes for hydrogen atoms (Table 3) are smaller than those of oxygen, nitrogen, and carbon atoms. As a result, the changes of C_Q properties for hydrogen atoms in different model systems are not so much significant compared to the change of other atoms. The results of C_Q properties for carbon atoms of C_{60} counterparts in hybrid systems show differences from each other and also from the original free C_{60} structure. However, the effects are significant for the atoms of interactions regions whereas the properties for atoms of other regions are almost remained unchanged. Careful examining of the results of C_Q properties for atom of investigated structures indicate that the effects of relaxations of MPO counterpart at the C_{60} surface are important because of significant changes of properties for some atoms in different cases of hybrids and also between separated and isolated forms. As a conclusion of this part, different magnitudes of C_Q properties for atoms of molecular counterparts in singular, separated, and hybrid cases show importance of monitoring of atomic electronic properties in molecular attachments.

CONCLUSIONS

The results of this work obtained by DFT based calculations for relaxations of original MPO and its tautomers at the C_{60} surfaces were explored to recognize electronic and structural properties for the considered model systems. Formations of tautomeric structures have significant effects on the electronic and structural properties of MPO structures. Moreover, tautomeric structures show different relaxations at the C_{60} surface referring to the characteristics properties for each model system. The total energies and corresponding deformation and binding energies indicate that the molecular properties are revised due to tautomerizations and relaxations at the C_{60} surfaces. Dipole moments also show that the polarities of model systems are altered in different structural cases based on the changes of properties for each tautomer. Atomic scale C_Q properties also indicated different electronic properties for atoms of tautomeric structures in

singular, separated and hybrid forms. Indeed, the effects are more significant for heavy atoms of oxygen, nitrogen and carbon atoms versus low-electron containing hydrogen atoms. Electronic sites of all atoms of the heterocyclic ring of MPO detect effects of tautomerizations and relaxations at the C_Q surfaces and the effects are significant for the interactions regions of C_{60} counterparts in the hybrid systems. And finally, the model systems indicated different types of relaxations, which could be a clue to visually recognize different tautomers of MPO structures by assistance of C_{60} substrate. Additionally, characteristic molecular and atomic properties could approve the correct observation of tautomeric structures.

ACKNOWLEDGEMENT

CONFLICT OF INTEREST

The authors declare that there is no conflict of interests regarding the publication of this manuscript.

REFERENCES

[1] Ma Y., Kong X., Abbate V., Hider R. C., (2015), Synthesis and characterization of novel iron specific bicyclic fluorescent probes. *Sens. Actuat. B*. 213: 12-19.

[2] Upanan S., Pangjit K., Uthaipibull C., Fucharoen S., McKie A. T., Srichairatanakool S., (2015), Combined treatment of 3–hydroxypyridine–4–one derivatives and green tea extract to induce hepcidin expression in iron–overloaded *β*–thalassemic mice. *Asian Pacific J. Trop. Biomed.* 5: 1010-1017.

[3] Andayi W. A., Egan T. J., Chibale K., (2014), Kojic acid derived hydroxypyridinone-chloroquine hybrids: Synthesis, crystal structure, antiplasmodial activity and *β*–haematin inhibition. *Bioorg. Med. Chem. Lett.* 24: 3263-3267.

[4] Medina-Franco J. L., Martínez–Mayorga K., Juárez–Gordiano C., Castillo R., (2007), Pyridin-2(1H)-ones: A promising class of HIV-1 non-nucleoside reverse transcriptase inhibitors. *Chem. Med. Chem.* 2: 1141-1147.

[5] De Clercq E., (2005), New approaches toward anti-HIV chemotherapy. *J. Med. Chem.* 48: 1297-1313.

[6] Reyes H., Aguirre G., Cháveza D., (2013), 4-Hydroxy-6-methylpyridin-2(1H)-one. *Acta Cryst. E*. 69: 1534-1538.

[7] Mohammadpour M., Zborowski K. K., Heidarpoor S., Żuchowski G., Proniewicz L. M., (2016), Modeling of stability and properties of anionic and cationic tautomers of the 3-hydroxypyridin-4-one system. *Comput. Theor. Chem.* 1078: 96-103.

[8] Yaraghi A., Ozkendir O. M., Mirzaei M., (2015), DFT studies of 5–fluorouracil tautomers on a silicon graphene nanosheet. *Superlatt. Microstruct.* 85: 784-788.

[9] Graff M., Dobrowolski J. C., (2013), On tautomerism of diazinones. *Comput. Theor. Chem.* 1026: 55-64.

[10] Siddiqui S. A., Bouarissa N., Rasheed T., Al–Assiri M. S., Al–Hajry A., (2014), Detection of electronically equivalent tautomers of adenine base: DFT study. *Mater. Res. Bull.* 51: 309-314.

[11] Garmaroudi F. S., Vahdati R. A. R., (2010), Functionalized CNTs for delivery of therapeutics. *Int. J. Nano Dimens.* 1: 89-102.

[12] Mirzaei M., (2013), Effects of carbon nanotubes on properties of the fluorouracil anticancer drug: DFT studies of a CNT-fluorouracil compound. *Int. J. Nano Dimens.* 3: 175-179.

[13] Mundra R. V., Wu X., Sauer J., Dordick J. S., Kane R. S., (2014), Nanotubes in biological applications. *Curr. Opin. Biotechnol.* 28: 25-32.

[14] Bodaghi A., Mirzaei M., Seif A., Giahi M., (2008), A computational NMR study on zigzag aluminum nitride nanotubes. *Physica E*. 41: 209-212.

[15] Rahimnejad S., Mirzaei M., (2011), Computational studies of planar, tubular and conical forms of silicon nanostructures. *Int. J. Nano Dimens.* 1: 257-260.

[16] Ahmadi R., Boroushaki T., Ezzati M., (2015), The usage comparison of occupancy parameters, gap band energy, ΔNmax at Xylometazoline medicine ratio its medical conveyer nano. *Int. J. Nano Dimens.* 6: 19-22.

[17] Ema M., Gamo M., Honda K., (2016), A review of toxicity studies of single–walled carbon nanotubes in laboratory animals. *Regul. Toxicol. Pharmacol.* 74: 42-63.

[18] Marmolejo–Tejada J. M., Velasco–Medina J., (2016), Review on graphene nanoribbon devices for logic applications. *Microelectron. J.* 48: 18-38.

[19] Linko V., Ora A., Kostiainen M. A., (2015), DNA nanostructures as smart drug–delivery vehicles and molecular devices. *Trends Biotechnol.* 33: 586-594.

[20] Rezvani M., Ganji M. D., Faghihnasiri M., (2013), Encapsulation of lamivudine into single walled carbon nanotubes: A vdW–DF study. *Physica E*. 52: 27-33.

[21] Mirzaei M., (2013), Uracil–functionalized ultra–small (n, 0) boron nitride nanotubes (n = 3–6): Computational studies. *Superlatt. Microstruct.* 57: 44-50.

[22] Ahmadian N., Ganji M. D., Laffafchy M., (2012), Theoretical investigation of nerve agent DMMP adsorption onto Stone–Wales defected single–walled carbon nanotube. *Mater. Chem. Phys.* 135: 569-574.

[23] Zhao J., Ma J., Nan X., Tang B., (2016), Application of non–covalent functionalized carbon nanotubes for the counter electrode of dye–sensitized solar cells. *Org. Electron.* 30: 52-59.

[24] Mirzaei M., (2013), Formation of a peptide assisted bi–graphene and its properties: DFT studies. *Superlatt. Microstruct.* 54: 47-53.

[25] Das T. P., Han E. L., (1958), Nuclear Quadrupole Resonance Spectroscopy. *Academic Press,* New York.

[26] Mirzaei M., Gulseren O., (2015), DFT studies of CNT-functionalized uracil–acetate hybrids. *Physica E*. 73: 105-109.

[27] Mirzaei M., Samadi Z., Hadipour N. L., (2010), Hydrogen bonds of peptide group in four acetamide derivatives: DFT study of oxygen and nitrogen NQR and NMR parameters. *J. Iran. Chem. Soc.* 7: 164-170.

[28] Seif A., Boshra A., Mirzaei M., Aghaie M., (2008), Carbon-substituting in (4, 4) boron nitride nanotube: Density functional study of boron-11 and nitrogen-14 electric field gradient tensors. *J. Theor. Comput. Chem.* 7: 447-455.

[29] Mirzaei M., Hadipour N. L., Abolhassani M. R., (2007), Influence of C-doping on the B-11 and N-14 quadrupole coupling constants in boron-nitride nanotubes: A DFT study. *Z. Naturforsch. A*. 62: 56-60.

[30] Mirzaei M., Elmi F., Hadipour N. L., (2006), A systematic investigation of hydrogen-bonding effects on the 17O, 14N, and 2H nuclear quadrupole resonance parameters of anhydrous and monohydrated cytosine crystalline structures: A density functional theory study. *J. Phys. Chem. B*. 110: 10991-10996.

[31] Pyykkö P., (2001), Spectroscopic nuclear quadrupole moments. *Mol. Phys.* 99: 1617-1629.

[32] Frisch M. J., Trucks G. W., Schlegel H. B., Scuseria G. E., Robb M. A., (2009), Gaussian 09, A.01. Gaussian Inc, *Pittsburgh,* PA.

[33] The Gaussian IOps Manual, www.gaussian.com/g_tech/g_iops/iops2.pdf.

[34] Grimme S., (2011), Density functional theory with London dispersion corrections. *WIREs Comput. Molec. Sci.* 1: 211-228.